COBEM 2021 26th International Congress of Mechanical Engineering
ABCM Associação Brasileira de Engenharia e Ciências Mecânicas
November 22-26, 2021, Virtual Congress, Brazil

COB-2021-0684
POST-FLUTTER ANALYSIS OF A NONLINEAR AEROELASTIC TYPICAL SECTION BASED ON THE METHOD OF MULTIPLE SCALES

José Augusto Ignácio da Silva[a]
j.i.silva@usp.br
Leonardo Sanches[b]
leonardo.sanches@isae-supaero.fr
Flávio D. Marques[a]
fmarques@sc.usp.br
[a] Department of Mechanical Engineering, São Carlos School of Engineering, University of São Paulo
j.i.silva@usp.br, fmarques@sc.usp.br
[b] Université de Toulouse, ICA, CNRS, ISAE-Supaero, Toulouse, France

Abstract. *Aeroelastic systems are susceptible to nonlinear behavior. The characterization of nonlinear response in aeroelastic systems is a relevant issue. It is essential to study the stability of the aeroelastic system under the effects of structural and aerodynamic nonlinearities to improve operational aircraft flight procedures. Bifurcation analysis is a benchmark approach to study the nonlinear post-flutter phenomenon. The current work presents an investigation on the dynamic behavior of three degrees of freedom typical section with nonlinear pitching stiffness, modeled by cubic and quintic polynomial terms. The unsteady aerodynamic loads are computed using the modified unsteady Theodorsen approximation for arbitrary motions. This investigation is based on the asymptotic analysis to be constructed by the method of multiple scales (MMS) to predict the nonlinear flutter onset and values of limit cycle oscillations (LCO) amplitudes at some post-flutter airspeed. Analytical Solutions for hardening and softening cases are constructed separately, and numerical simulations reveal that MMS can accurately predict super-critical and sub-critical bifurcations for both scenarios.*

Keywords: *Aeroelastic typical section, Post-flutter, Nonlinear pitching stiffness, Method of multiple scales, Super-critical and sub-critical bifurcations.*

1. INTRODUCTION

Concentrated structural nonlinearities are commonly present in aeroelastic systems inducing different behavior to the response of flight vehicles. Among the typical nonlinear response phenomena, one may observe multiple fixed points, bifurcations, limit cycles oscillations (LCOs), instabilities, and chaos (Lee *et al.*, 1999). Nonlinear responses can suffer from abrupt changes from damped motions to LCOs, which limits the operational regime of aircraft and may result in structural fatigue, or even to catastrophic failure. Sources of these nonlinearities are generally geometrical (i.e., related to large structural deflections) or material physics characteristics, and those effects can be incorporated into aeroelastic models through the elastic restoring and damping forces or moments representations. The most used concentrated structural nonlinearities representations are the hardening or softening stiffness, free-play, dry-friction, quadratic damping and hysteresis (Dimitriadis, 2017).

Many technical contributions have been reported along the years involving the analysis of aeroelastic systems with structural nonlinearities. Lee *et al.* (2005) applied the harmonic balance method (HBM) to analyze the bifurcation behavior of a pitch-plunge airfoil with cubic stiffness in the pitching motion. Conner *et al.* (1997) presented an important investigation about the dynamic behavior of a typical airfoil section with control surface free-play. The experimental validation of free-play induce LCOs were carried out by Refs. (Trickey *et al.*, 2002; Vasconcellos *et al.*, 2012). Recently, the effect of multiple combined concentrated nonlinearities have been investigated by the Refs. (Pereira *et al.*, 2016; da Silva and Marques, 2021)

The dynamic characterization of nonlinear aeroelastic systems by means analytic asymptotic methods is a promising topic that has been attained a great interest of the scientific community. Besides the quick access of bifurcation diagrams, LCOs amplitudes and its stability, these approaches make it possible the rapid parametric analysis, tailoring and re-design of aeroelastic structures. In this sense, Abdelkefi *et al.* (2012) employed normal form of the Hopf bifurcation to compute the sub-critical behavior induced by pitch free-play in a two degrees of freedom (*dof*) airfoil. Sanches *et al.* (2019) used the method of multiple scales (MMS) to predict the nonlinear flutter boundary of an airfoil with a control surface considering pitch cubic stiffness.

Typically hardening geometric nonlinearities in pitch airfoil motion is modeled by a cubic stiffness term. However,

any times the results covered by this modelling diverge with those obtained experimentally as the existence of sub-critical bifurcation behavior (Pereira *et al.*, 2016), which is inconsistent according with nonlinear aeroelastic theory. In this sense, this paper introduces a quintic order polynomial function for modeling a geometric nonlinearity in pitch-*dof* of an aeroelastic typical section with control surface. This representation allows to access both hardening and softening scenarios that converge with experimental realizations. Analytical solutions to predict the bifurcation behavior of the aeroelastic system for both cases are built based on the method of multiple scales (MMS). The obtained results are validated with those found by direct numerical time integration of the model. After, a complete parametric analysis is performed to show the effect of each restoring nonlinear coefficient in the dynamic behavior of the aeroelastic system.

2. NONLINEAR TYPICAL AEROELASTIC SECTION MODELING

The aeroelastic typical section assumed in this paper is illustrated in Figure 1. The model consists of a two dimensional airfoil with the semi-chord length of b, mass per span length m, mass inertia moment I_α and a static moment S_α, and three-*dof*, namely, plunge, pitch and control surface deflection. The plunge motion is denoted by $h(t)$ (positive downwards), the pitch by $\alpha(t)$ (positive clockwise), and the control surface angular deflection by $\beta(t)$ (positive clockwise). A reference coordinate system is placed with origin at the airfoil mid-chord.The elastic suspension composed by concentrated spring stiffness, k_α and k_h, limits the airfoil motion in pitch and plunge, respectively, at the so-called elastic axis, which is positioned at ab from the reference system origin. The control surface has a mass inertia moment I_β and a static moment S_β and its deflection (measured in the hinge at cb from mid-chord) is restrained to the airfoil structure by a spring of k_β stiffness value. The structural damping effect is omitted in order capture more critical instabilities. The center of gravity positions of the airfoil (CG_a) and control surface (CG_s) are measured from the elastic axis (bx_α) and hinge point (bx_β), respectively. Under the influence of aerodynamic flow with airspeed U, the typical section unsteady loading comprises the lift force ($L(t)$), pitching moment at the elastic axis ($M_\alpha(t)$), and the control surface hinge moment ($M_\beta(t)$).

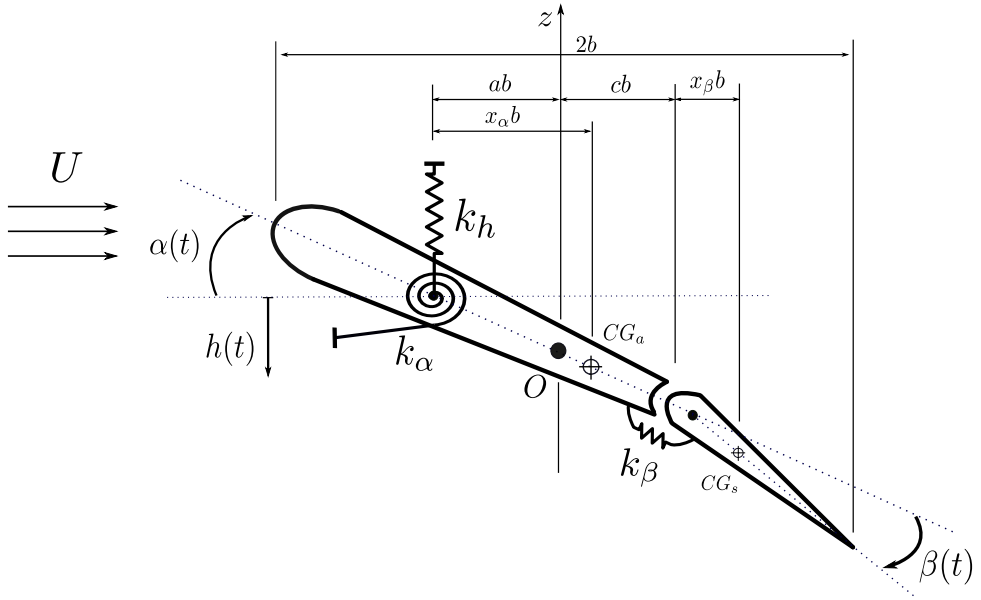

Figure 1. Sketch of a typical aeroelastic section.

The aeroelastic equations of motion can be derived using the Lagrange's equations (Fung, 1969), and conveniently written in the following dimensionless form:

$$\begin{cases} \ddot{\xi}(t) + x_\alpha\ddot{\alpha}(t) + x_\beta\ddot{\beta}(t) + \omega_h^2\xi(t) = -L(t)/mb \\ r_\alpha^2\ddot{\alpha}(t) + (r_\beta^2 + (c-a)x_\beta)\ddot{\beta}(t) + x_\alpha\ddot{\xi}(t) + r_\alpha^2\omega_\alpha^2\alpha(t) + r_\alpha^2\omega_\alpha^2 F_\alpha(\alpha(t)) = M_\alpha(t)/mb^2 \\ r_\beta^2\ddot{\beta}(t) + (r_\beta^2 + (c-a)x_\beta)\ddot{\alpha}(t) + x_\beta\ddot{\xi}(t) + r_\beta^2\omega_\beta^2\beta(t) = M_\beta(t)/mb^2 \end{cases} \tag{1}$$

where $\xi(t) = h(t)/b$ is the dimensionless plunge motion, $x_\alpha = S_\alpha/mb$, $x_\beta = S_\beta/mb$ are the dimensionless distances from the elastic axis to the airfoil center of gravity (CG_a) and from the control surface hinge to its (CG_s), respectively, $r_\alpha^2 = I_\alpha/mb^2$ and $r_\beta^2 = I_\beta/mb^2$ are the radii of gyration of the airfoil and trailing edge control surface, $\omega_h^2 = k_h/m$, $\omega_\alpha^2 = k_\alpha/I_\alpha$ and $\omega_\beta^2 = k_\beta/I_\beta$ are the plunge, pitch and control surface uncoupled natural frequencies, respectively. The function $F_\alpha(\alpha)$ refers to the geometric structural nonlinearity considered in the pitch stiffness, that can assumes the following quintic polynomial form:

$$F_\alpha(\alpha(t)) = C_\alpha\alpha^3(t) + Q_\alpha\alpha^5(t) \tag{2}$$

where C_α and Q_α are the cubic and quintic coefficients used to adjust the data obtained with the static restoring experiment. For positive values of both parameters, this function can represent a hardening nonlinearity and, for negative values of C_α, the softening scenario is achieved. More details about this modeling can be addressed in Pidaparthi and Missoum (2019).

The unsteady aerodynamic model used to compute $L(t)$, $M_\alpha(t)$, and $M_\beta(t)$ is linear and based on a generalization of Theodorsen's approach (Theodorsen, 1935) for harmonic aerodynamic loading, where the Theodorsen function of reduced frequency can be expanded using the relation with the indicial response by the Wagner function. After applying the Padé polynomial interpolation, a formulation that leads to augmented aerodynamic states is achieved (Vasconcellos *et al.*, 2012). The final set of aeroelastic equations of motion becomes:

$$\begin{cases} (\mathbf{M}_s - \mathbf{M}_{nc})\,\ddot{\mathbf{x}}_s(t) - (\mathbf{B}_{nc} + \mathbf{B}_c)\,\dot{\mathbf{x}}_s(t) + (\mathbf{K}_s - \mathbf{K}_{nc} - \mathbf{K}_c)\,\mathbf{x}_s(t) - \mathbf{A}_1\dot{\bar{x}}(t) - \mathbf{A}_2\bar{x}(t) + \mathbf{f}_{nl}(\mathbf{x}_s(t)) = \mathbf{0} \\ \ddot{\bar{x}}(t) - \mathbf{A}_5\dot{\bar{x}}(t) - \mathbf{A}_6\bar{x}(t) - \mathbf{A}_3\dot{\mathbf{x}}_s(t) - \mathbf{A}_4\mathbf{x}_s(t) = \mathbf{0} \end{cases} \tag{3}$$

where $\mathbf{x}_s(t) = [\xi(t) \;\; \alpha(t) \;\; \beta(t)]^T$ is the vector of displacements, $\bar{x}(t)$ is the augmented aerodynamic state, $\mathbf{M}_s$, and $\mathbf{K}_s$ are the structural inertia and stiffness matrices, respectively, $\mathbf{f}_{nl}(\mathbf{x}_s(t))$ is the vector of structural nonlinearities, $\mathbf{M}_{nc}$, $\mathbf{B}_{nc}$ and $\mathbf{K}_{nc}$ are the respective non-circulatory aerodynamic matrices related to inertia, damping and stiffness, $\mathbf{B}_c$ and $\mathbf{K}_c$ are the respective circulatory aerodynamic matrices related to damping and stiffness, and $\mathbf{A}_i$ (for $i = 1, \ldots, 6$) are the augmented aerodynamic matrices. Matrices in Eq. (3) are detailed in Appendix A.

Equations (3) can be conveniently compacted at the following matrix form:

$$\mathbf{M}_t\ddot{\boldsymbol{\chi}}(t) + \mathbf{B}_t(U)\dot{\boldsymbol{\chi}}(t) + \mathbf{K}_t(U)\boldsymbol{\chi}(t) + \epsilon\hat{\mathbf{F}}_{nl}(\boldsymbol{\chi}(t)) = \mathbf{0} \tag{4}$$

where $\boldsymbol{\chi}(t) = [\xi(t) \;\; \alpha(t) \;\; \beta(t) \;\; \bar{x}(t)]^T$ is the vector of *dof*'s, $\mathbf{M}_t$, $\mathbf{B}_t(U)$ and $\mathbf{K}_t(U)$ are the total (structural and aerodynamic) inertia, damping and stiffness matrices, respectively, $\mathbf{F}_{nl}(\boldsymbol{\chi}(t)) = \begin{bmatrix} 0 & r_\alpha^2\omega_\alpha^2(\hat{C}_\alpha\alpha^3(t) + \hat{Q}_\alpha\alpha^5(t)) & 0 & 0 \end{bmatrix}^T$, with $\hat{C}_\alpha = C_\alpha/\epsilon$ and $\hat{Q}_\alpha = Q_\alpha/\epsilon$. In addition, ϵ represents a small real-valued constant (< 1.0) that scales the system's nonlinearities for the asymptotic with MMS. Matrices in Eq. (4) are also given in the Appendix A.

3. ASYMPTOTIC DYNAMIC ANALYSIS WITH METHOD OF MULTIPLE SCALES

The Method of Multiple Scales (MMS) is employed to capture the effect of nonlinearities on the limit-cycle oscillations amplitude, its stability and the nonlinear flutter envelope through analytical expressions. Regarding the aeroelastic model, it is assumed a perturbation on the neighborhood of critical flutter airspeed (U_c) of the associated linear system, as the following:

$$U = U_c + \epsilon\sigma \tag{5}$$

where σ is a perturbation parameter on the critical airspeed. Since the damping and stiffness matrices depend on the airspeed (U), they can be decomposed into:

$$\begin{cases} \mathbf{B}_t(U) = \mathbf{B}_{t_0}(U_c) + \epsilon\sigma\mathbf{B}_{t_1}(U_c) \\ \mathbf{K}_t(U) = \mathbf{K}_{t_0}(U_c) + \epsilon\sigma\mathbf{K}_{t_1}(U_c) \end{cases} \tag{6}$$

where $\mathbf{B}_{t_j}(U_c) = \partial^j\mathbf{B}_t/\partial U^j|_{U=U_c}$ and $\mathbf{K}_{t_j}(U_c) = \partial^j\mathbf{K}_t/\partial U^j|_{U=U_c}$, with $j = 0, 1$. The MMS assumes the following expansion of the generalized coordinates (Nayfeh and Mook, 1995):

$$\boldsymbol{\chi}(t) = \boldsymbol{\chi}_0(T_0, T_1) + \epsilon\boldsymbol{\chi}_1(T_0, T_1) \tag{7}$$

with, T_0 and T_1 being the fast and slow time scales. Introducing Eqs. (6), (7) in Eq. (4), results in two set of equations for ϵ^0 and ϵ^1, given as following,

ϵ^0:

$$\mathbf{M}_t\frac{\partial^2(\boldsymbol{\chi}_0)}{\partial T_0^2} + \mathbf{B}_{t_0}\frac{\partial(\boldsymbol{\chi}_0)}{\partial T_0} + \mathbf{K}_{t_0}\boldsymbol{\chi}_0 = \mathbf{0} \tag{8}$$

ϵ^1:

$$\mathbf{M}_t\frac{\partial^2(\boldsymbol{\chi}_1)}{\partial T_0^2} + \mathbf{B}_{t_0}\frac{\partial(\boldsymbol{\chi}_1)}{\partial T_0} + \mathbf{K}_{t_0}\boldsymbol{\chi}_1 = -2\mathbf{M}_t\frac{\partial^2(\boldsymbol{\chi}_0)}{\partial T_1\partial T_0} - \mathbf{B}_{t_0}\frac{\partial(\boldsymbol{\chi}_0)}{\partial T_1} - \sigma\mathbf{B}_{t_1}\frac{\partial(\boldsymbol{\chi}_0)}{\partial T_0} - \sigma\mathbf{K}_{t_1}\boldsymbol{\chi}_0 - \hat{\mathbf{F}}_{nl}(\boldsymbol{\chi}_0) \tag{9}$$

The set of ϵ^0 equations correspond to the associated linear aeroelastic problem of Eq. (4), which according with Center Manifold Theorem (Luongo and Zulli, 2014), can assume the following solution:

$$\boldsymbol{\chi}_0(T_0,T_1) = C(T_1)\mathbf{u}e^{j\omega_c T_0} + \overline{C}(T_1)\overline{\mathbf{u}}e^{-j\omega_c T_0} \tag{10}$$

where $C(T_1)$ and ω_c are the slowly modulated complex amplitude and angular frequency of critical mode, respectively, $j=\sqrt{-1}$ is the imaginary unity, and the over-bar $\overline{(\,)}$ indicates complex-conjugate. Substituting Eq. (10) in Eq. (8), leads to the following right and left eigenvalue problem (Luongo and Zulli, 2014):

$$\left(\lambda^2\mathbf{M}_t + \lambda\mathbf{B}_{t_0} + \mathbf{K}_{t_0}\right)\mathbf{u} = \mathbf{0}, \qquad \left(\overline{\lambda}^2\mathbf{M}_t^T + \overline{\lambda}\mathbf{B}_{t_0}^T + \mathbf{K}_{t_0}^T\right)\mathbf{v} = \mathbf{0}, \tag{11}$$

where $\lambda = \pm j\omega_c$ is the eigenvalue related to the right ($\mathbf{u} = [u_1 \;\; u_2 \;\; u_3 \;\; u_4]^T$) and left eigenvectors ($\mathbf{v} = [v_1 \;\; v_2 \;\; v_3 \;\; v_4]^T$), respectively, of the critical mode. By inserting Eq. (10) in Eq. (9), the ϵ^1- order problem can be rewritten as:

$$\begin{aligned}&\mathbf{M}_t\frac{\partial^2\boldsymbol{\chi}_1}{\partial T_0^2} + \mathbf{B}_{t_0}\frac{\partial\boldsymbol{\chi}_1}{\partial T_0} + \mathbf{K}_{t_0}\boldsymbol{\chi}_1 = \\ &\left[-(2j\omega_c\mathbf{M}_t\mathbf{u} + \mathbf{B}_{t_0}\mathbf{u})\frac{\partial C}{\partial T_1} - (j\omega_c\mathbf{B}_{t_1}\mathbf{u} + \mathbf{K}_{t_1}\mathbf{u})\sigma C - 3\mathbf{f}_1C^2\overline{C} - 10\mathbf{f}_2C^3\overline{C}^2\right]e^{j\omega_c T_0} + [N.S.T.] + [c.c.]\end{aligned} \tag{12}$$

where $\mathbf{f}_1(u_2,u_2,\overline{u}_2) = \left[0 \;\; r_\alpha^2\omega_\alpha^2\hat{C}_\alpha u_2^2\overline{u}_2 \;\; 0 \;\; 0\right]^T$ and $\mathbf{f}_2(u_2,u_2,u_2,\overline{u}_2,\overline{u}_2) = \left[0 \;\; r_\alpha^2\omega_\alpha^2\hat{Q}_\alpha u_2^3\overline{u}_2^2 \;\; 0 \;\; 0\right]^T$, $[c.c.]$ indicates complex-conjugate, and $[N.S.T.]$ represents the nonsecular terms. The terms with the same frequency of the critical mode (ω_c) are the so-called secular terms, which is matching to zero to avoid divergent solutions. The solvability condition for the asymptotic expansion is reached by pre-multiplying the seculars terms by the hermitian left eigenvectors ($\mathbf{v}^H$) (Luongo and Zulli, 2014), which leads to:

$$\Gamma_1\frac{\partial C}{\partial T_1} = \Gamma_2\sigma C + \Gamma_3 C^2\overline{C} + \Gamma_4 C^3\overline{C}^2, \quad \text{with} \;\; \Gamma_1 = 2j\omega_c\mathbf{v}^H\mathbf{M}_t\mathbf{u} + \mathbf{v}^H\mathbf{B}_{t_0}\mathbf{u}, \;\; \Gamma_2 = -j\omega_c\mathbf{v}^H\mathbf{B}_{t_1}\mathbf{u} - \mathbf{v}^H\mathbf{K}_{t_1}\mathbf{u},$$

$$\Gamma_3 = -3r_\alpha^2\omega_\alpha^2\hat{C}_\alpha u_2^2\overline{u}_2\overline{v}_2, \;\; \Gamma_4 = -10r_\alpha^2\omega_\alpha^2\hat{Q}_\alpha u_2^3\overline{u}_2^2\overline{v}_2. \tag{13}$$

4. BIFURCATION AND LIMIT CYCLE OSCILLATION ANALYSIS

The Hopf bifurcation analysis of the nonlinear aeroelastic model is carried out by studying the evolution of equilibrium responses (i.e., LCO amplitude and its stability) as a function of the parameter σ. Under this purpose, the complex amplitude $C(T_1)$ can be written in the polar form, as the following (Nayfeh and Mook, 1995):

$$C(T_1) = \frac{1}{2}a(T_1)e^{j\beta(T_1)} \tag{14}$$

where, $a(T_1)$ and $\beta(T_1)$ are the amplitude and phase of the critical vibration mode at the time scale T_1. In this approach, the phase could be not captured, however, Berci and Dimitriadis (2018) discuss the necessity of considering high-order terms in the MMS approach to predict it.

Substituting Eq. (14) into Eq. (13), the modulated amplitude equation can be achieved, such as:

$$\frac{\partial a}{\partial T_1} = \frac{\mathcal{R}e\{\Gamma_2\}}{\mathcal{R}e\{\Gamma_1\}}\sigma a + \frac{\mathcal{R}e\{\Gamma_3\}}{\mathcal{R}e\{\Gamma_1\}}a^3 + \frac{\mathcal{R}e\{\Gamma_4\}}{\mathcal{R}e\{\Gamma_1\}}a^5, \;\; \text{if} \;\; \mathcal{R}e\{\Gamma_1\} \neq 0. \tag{15}$$

The LCOs amplitude is calculated by determining the steady-state amplitude (i.e., when $\frac{\partial a}{\partial T_1} = 0$ and $a = a_E$), which is analytically computed through:

$$a_E = \left[0, \;\; \pm\sqrt{r}\right], \tag{16}$$

where r are the real-solutions of the polynomial equation, $\mathcal{R}e\{\Gamma_4\}r^2 + \mathcal{R}e\{\Gamma_3\}r + \sigma\mathcal{R}e\{\Gamma_2\} = 0$, given by:

$$r = \frac{-\mathcal{R}e\{\Gamma_3\} \pm \sqrt{\mathcal{R}e\{\Gamma_3\}^2 - 4\mathcal{R}e\{\Gamma_2\}\mathcal{R}e\{\Gamma_4\}}}{2\mathcal{R}e\{\Gamma_4\}}, \qquad \text{if} \;\; \mathcal{R}e\{\Gamma_3\}^2 - 4\mathcal{R}e\{\Gamma_2\}\mathcal{R}e\{\Gamma_4\} > 0 \tag{17}$$

The stability of these steady-state amplitudes can be studied by considering small deviations ($\delta a(T_1)$) from the equilibrium response (a_E). Therefore, from Eq. (15), it comes:

$$\frac{\partial}{\partial T_1}(\delta a(T_1)) = \left(\frac{\mathcal{R}e\{\Gamma_2\}}{\mathcal{R}e\{\Gamma_1\}}\sigma + 3\frac{\mathcal{R}e\{\Gamma_3\}}{\mathcal{R}e\{\Gamma_1\}}a_E^2 + 5\frac{\mathcal{R}e\{\Gamma_4\}}{\mathcal{R}e\{\Gamma_1\}}a_E^4\right)\delta a(T_1), \tag{18}$$

since the higher order terms are neglected. The LCO amplitudes computed through Eq. (16) are stable if positive value is attained in the right-hand side of Eq. (18). Otherwise, the motion is unstable. The knowledge of the amplitude and stability of LCOs are very important to characterize super- and sub-critical bifurcations of the aeroelastic system.

5. RESULTS AND DISCUSSION

The aeroelastic system was analyzed for each nonlinear scenario (hardening and softening), using the following aeroelastic typical section parameters: $b = 0.5$ m, $a = -0.5$, $c = 0.5$, $\omega_h = 4\pi$ rad/s, $\omega_\alpha = 8\pi$ rad/s, $\omega_\beta = 20\pi$ rad/s, $x_\alpha = 0.5$, $x_\beta = 0.003$, $r_\alpha = 0.75$, $r_\beta = 0.008$, $\rho = 1.0$ kg/m^3, $m = 15.708$ kg (Sanches *et al.*, 2019). Before the nonlinear analysis, a linear stability inspection of the aeroelastic system (i.e., $F_\alpha(\alpha(t)) = 0$) was carried out. The evolution of the system's eigenvalues with the airspeed U is depicted in Figure 2(a). The linear flutter phenomenon is detected when the real part of the eingenvalues reaches zero. Therefore, the critical flutter airspeed is $U_c = 33.3$ m/s. This airspeed also characterizes the stability limits, where the aeroelastic system will change from stable damped responses to unstable behavior. Figure 2(b) shows the evolution of the eigenfrequencies with airspeed U. At the flutter condition, the frequency of the critical mode of vibration is $\omega_c = 17.83$ rad/s, in addition, its right and left eigenvectors are given by $\mathbf{u} = [0.032269 + 0.023814j \;\; 0.0010901 - 0.023810j \;\; 0.027904 + 0.023073j \;\; 0.0013829 - 0.0043897j]^T$ and $\mathbf{v} = [0.031293 + 0.0025574j \;\; 0.47689 - 0.152311j \;\; -0.032659 + 0.016416j \;\; 0.048331 + 0.021802j]^T$.

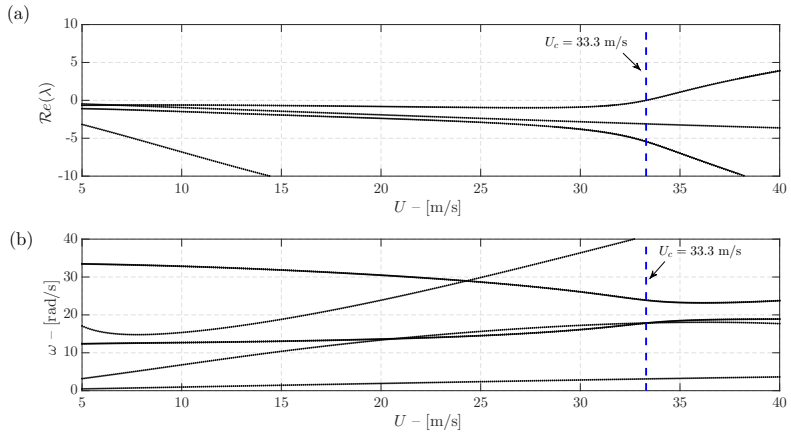

Figure 2. Linear flutter analysis: (a) variation of the damping ratios with the airspeed U and (b) variation of the eigenfrequencies with the airspeed U.

5.1 Validation of Analytical Approach

To validate the present approach, hardening and softening nonlinear scenarios are considered, for that, bifurcation diagrams (LCO amplitude over airspeed U) are building and compared with those obtained via numerical integration of the model. The fourth-order Runge-Kutta method with a time step of a 10^{-3} seconds is used to simulate the aeroelastic equations of motion in Equation (3), considering each nonlinear scenario. For all simulated cases, an arbitrary initial condition of $\boldsymbol{\chi}(0) = \begin{bmatrix}10^{-2} & 1^\circ & 0.1^\circ & 0 & 0 & 0 & 0 & 0\end{bmatrix}^T$ is adopted. In order to have a better numerical understanding of the nonlinear behavior of the aeroelastic system, the simulation considers several time windows, in which the airspeed is kept constant. Each window had a time span equal to 100 seconds. For a time window to another, the airspeed is varied by steps of 0.1 m/s, following an increasing in U up to a maximum value, and after that it decreases until reaching back the initial airspeed value. To ensure that the steady-state LCO was reached (i.e., no transient effects), the amplitude values for the bifurcation diagram construction were taken in the last 5 seconds of each respective simulation window. Figure 3 depicts the bifurcation diagram for the hardening scenario, considering $C_\alpha = 3$ and $Q_\alpha = 20$. The results reveals a supercritical bifurcation behavior, highlighted by stable LCOs. Figure 4 shows the bifurcation analysis of the softening case, considering $C_\alpha = -3$ and $Q_\alpha = 20$. Based on this analysis, it is verified that the softening nonlinear effect induces the existence of LCOs in airspeed below the Hopf bifurcation point (i.e., the linear flutter onset point U_c), which characterizes a sub-critical bifurcation behavior, highlighted by unstable LCOs. It is also verified that the softening condition induces more high LCOs amplitudes in post-critical flutter regime than hardening ones. Figure 5(a,b) shows time histories plots at $U/U_c = 1.03$ for hardening and softening nonlinear cases, respectively. Based on these results, it is observed a good agreement between the analytical (MMS) and numerical solutions near the critical flutter airspeed, where the accuracy of this method can degenerate at airspeed so far from it.

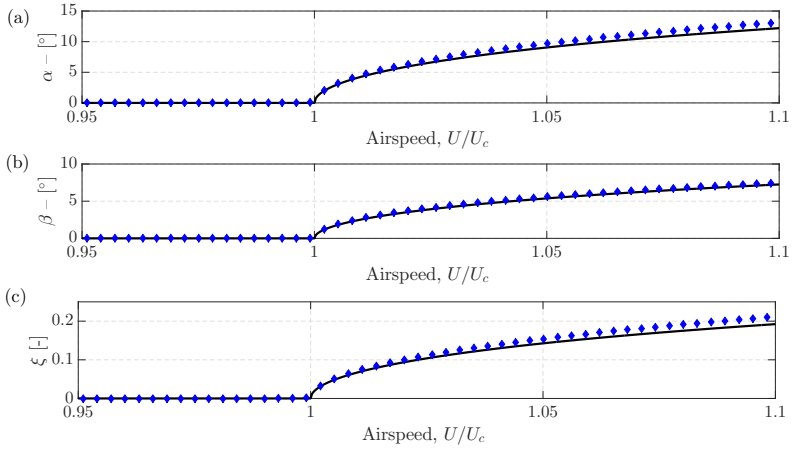

Figure 3. Bifurcation analysis for the hardening scenario, considering $C_\alpha = 3$ and $Q_\alpha = 20$: (a) pitch, (b) control surface, (c) plunge. —— stable LCOs via MMS, ♦ run-up.

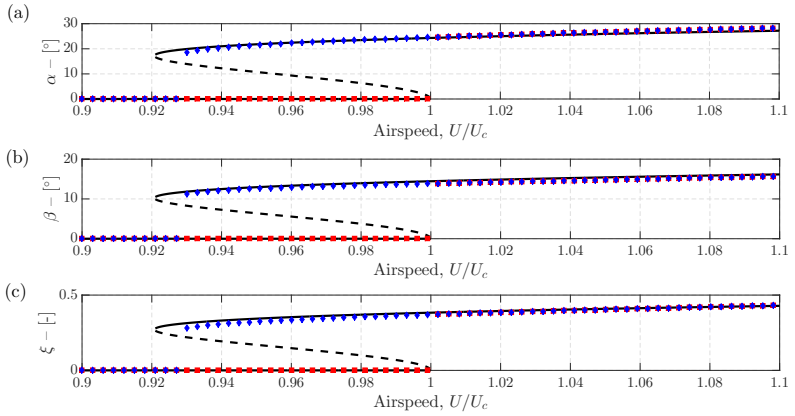

Figure 4. Bifurcation analysis for the softening scenario, considering $C_\alpha = -3$ and $Q_\alpha = 20$: (a) pitch, (b) control surface, (c) plunge. —— stable via MMS, - - - unstable via MMS, ■ run-up, ♦ run-down.

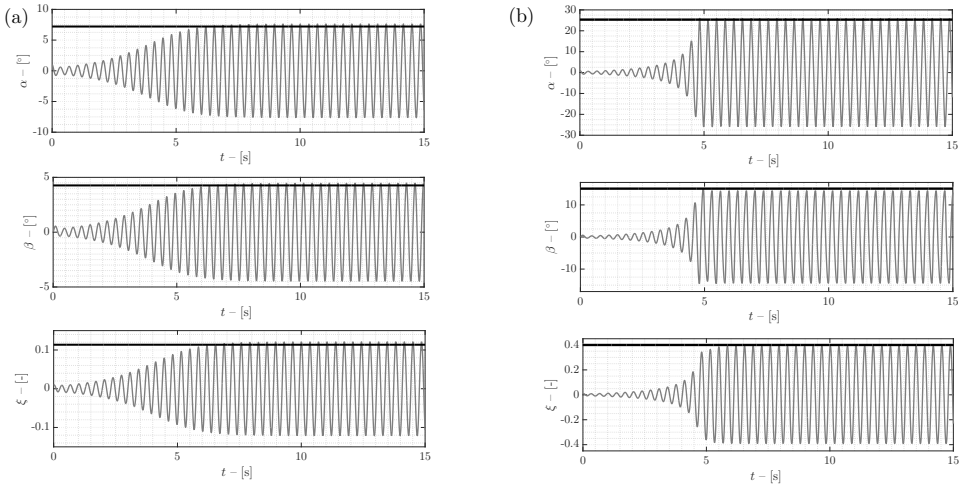

Figure 5. Time histories at $U/U_c = 1.03$: (a) hardening scenario ($C_\alpha = 3$, $Q_\alpha = 20$), (b) softening scenario ($C_\alpha = -3$, $Q_\alpha = 20$). —— numerical integration, —— MMS.

5.2 Parametric Analysis

In order to explore the effect of cubic and quintic pitch restoring terms for both hardening and softening scenarios, a complete parametric analysis is carried out. In respect to hardening scenario, Figure 6(a) depicts the amplitudes of the limit cycle oscillations for each of the three-*dof* motion. Here, the quintic parameter is fixed with the value of $Q_\alpha = 20$

and the cubic term (C_α) can vary. Based on the parametric analysis, it is verified that the post-critical LCO amplitude reduces significantly with the increase of cubic parameter. Similarly, Figure 6(b) analyzes the impact of the quintic term (Q_α), considering the cubic coefficient fixed in $C_\alpha = 3.0$. This result reveals that increasing C_α slightly reduces the motion amplitudes. It is also verified that both cubic and quintic coefficients no plays important effect on the LCOs stability.

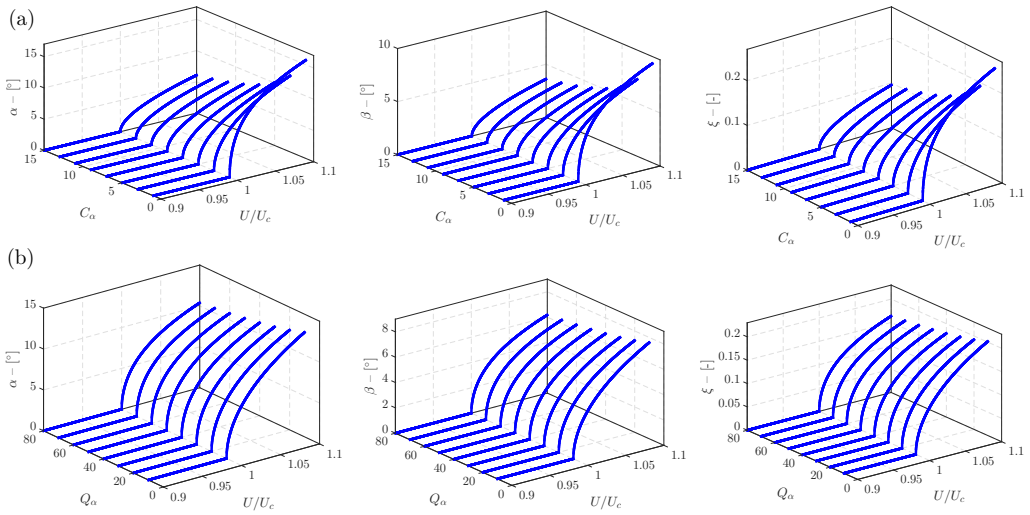

Figure 6. Parametric bifurcation analysis for hardening scenario: (a) effect of cubic term (C_α), considering $Q_\alpha = 20$, (b) effect of quintic term (Q_α), considering $C_\alpha = 3$. —— stable.

Regarding the softening scenario, Figure 7(a) shows the effect of cubic coefficient in the system's bifurcation, considering $Q_\alpha = 20$. Based on this analysis, it is verified that more negative values of C_α can anticipate the presence of LCOs at airspeed below the critical flutter, which expand the range of unstable motions and limits the flight envelope. Higher amplitudes are also observed for these LCOs. In Figure 7(b), the impact of quintic coefficient is studied, considering $C_\alpha = -3$. Based on this result, it is verified that more higher values of Q_α can alleviate the LCOs amplitudes and assure the system's stability, reducing significantly the range of unstable motions.

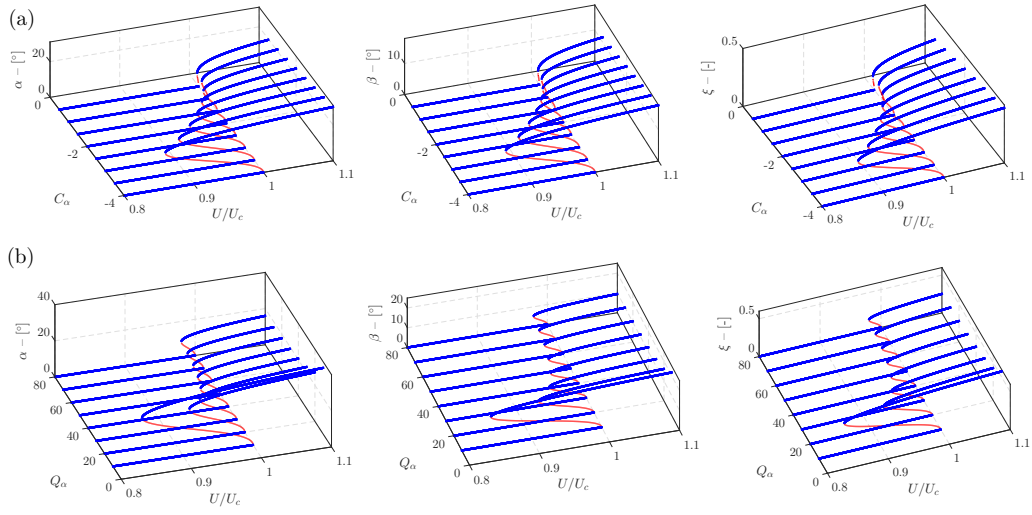

Figure 7. Parametric bifurcation analysis for softening scenario: (a) effect of cubic term (C_α), considering $Q_\alpha = 20$, (b) effect of quintic term (Q_α), considering $C_\alpha = -3$. —— stable, ····· unstable.

6. CONCLUDING REMARKS

This paper presented a dynamic characterization of a typical aeroelastic section with the trailing edge control surface under the influence of structural concentrated nonlinearities. The aeroelastic model is based on the conventional three-*dof* airfoil where the geometric concentrated nonlinearity is considered in the pitching motion, by including a quintic polynomial stiffness. Hardening and softening scenarios are considered in this investigation. A linear unsteady aerodynamic

loading model is adopted to assess the aeroelastic equations of motion. The method of multiple scales is used to build analytical solutions capable to predict the aeroelastic bifurcations, LCOs amplitudes and its stability. After the validation of presented method a parametric study of the nonlinear coefficients was also carried out.

The simulations and bifurcation results reveal that MMS is capable to predict accurately the pre- and post-critical nonlinear flutter phenomenon for both hardening and softening scenarios. Aside the efficient prediction of LCOs amplitudes and stability, this approach is computationally more efficient than numerical approaches.

Regarding the parametric analysis, it is observed that for the hardening scenario the increase of cubic and quintic nonlinear restoring coefficients are beneficial for the flight envelope, once results in a attractive reduction of LCO amplitudes and no impacts the system's stability. For the softening scenario, it is observed that larger negative values of cubic coefficient can degenerate the aeroelastic stability of the system and also inducing higher LCOs amplitudes. On the other hand, the increase of quintic coefficient in this scenario is so beneficial for the aeroelastic stability and amplitude LCO mitigation.

Therefore, by combining the appropriate parameters regarding the cubic and quintic coefficients in an aeroelastic tailoring scheme, it is possible to mitigate the undesirable sub-critical bifurcation behavior. Such an approach may improve design criteria for allowed mild nonlinear behavior in aeroelastic systems.

7. ACKNOWLEDGEMENTS

The authors acknowledge the financial support from the São Paulo Research Foundation (FAPESP grant #2019/05410–9) and the National Council for Scientific and Technological Development (CNPq grant #306824/2019–1).

8. REFERENCES

Abdelkefi, A., Vasconcellos, R., Marques, F. and Hajj, M., 2012. "Modeling and identification of freeplay nonlinearity". *Journal of Sound and Vibration*, Vol. 331, No. 8, pp. 1898 – 1907. ISSN 0022-460X. doi:10.1016/j.jsv.2011.12.021.

Berci, M. and Dimitriadis, G., 2018. "A combined multiple time scales and harmonic balance approach for the transient and steady-state response of nonlinear aeroelastic systems". *Journal of Fluids and Structures*, Vol. 80, pp. 132–144. doi:10.1016/j.jfluidstructs.2018.03.003.

Conner, M., Tang, D., Dowell, E. and Virgin, L., 1997. "Nonlinear behavior of a typical airfoil section with control surface freeplay: A numerical and experimental study". *Journal of Fluids and Structures*, Vol. 11, No. 1, pp. 89 – 109. ISSN 0889-9746. doi:10.1006/jfls.1996.0068.

da Silva, J.A.I. and Marques, F.D., 2021. "Characterization of typical aeroelastic sections under combined structural concentrated nonlinearities". *Journal of Vibration and Control*. doi:10.1177/2F10775463211000161.

Dimitriadis, G., 2017. *Introduction to Nonlinear Aeroelasticity*. John Wiley & Sons Ltd.

Fung, Y.C., 1969. *An Introduction to the Theory of Aeroelasticity*. Dover Publications, INC, New York.

Lee, B., Liu, L. and Chung, K., 2005. "Airfoil motion in subsonic flow with strong cubic nonlinear restoring forces". *Journal of Sound and Vibration*, Vol. 281, No. 3, pp. 699 – 717. ISSN 0022-460X. doi:10.1016/j.jsv.2004.01.034.

Lee, B., Price, S. and Wong, Y., 1999. "Nonlinear aeroelastic analysis of airfoils: bifurcation and chaos". *Progress in Aerospace Sciences*, Vol. 35, pp. 205–334. doi:10.1016/S0376-0421(98)00015-3.

Luongo, A. and Zulli, D., 2014. "Aeroelastic instability analysis of NES-controlled systems via a mixed multiple scale/harmonic balance method". *Journal of Vibration and Control*, Vol. 20, No. 13, pp. 1985–1998. doi: 10.1177/1077546313480542.

Nayfeh, A.H. and Mook, D.T., 1995. *Nonlinear Oscillations*. John Wiley & Sons Ltd.

Pereira, D.A., Vasconcellos, R.M., Hajj, M.R. and Marques, F.D., 2016. "Effects of combined hardening and free-play nonlinearities on the response of a typical aeroelastic section". *Aerospace Science and Technology*, Vol. 50, pp. 44 – 54. ISSN 1270-9638. doi:10.1016/j.ast.2015.12.022.

Pidaparthi, B. and Missoum, S., 2019. "Stochastic optimization of nonlinear energy sinks for the mitigation of limit cycle oscillations". *AIAA Journal*, Vol. 57, No. 5, pp. 2134–2144. doi:10.2514/1.J057897.

Sanches, L., Guimarães, T.A. and Marques, F.D., 2019. "Aeroelastic tailoring of nonlinear typical section using the method of multiple scales to predict post-flutter stable LCOs". *Aerospace Science and Technology*, Vol. 90, pp. 157 – 168. ISSN 1270-9638. doi:10.1016/j.ast.2019.04.031.

Theodorsen, T., 1935. "General theory of aerodynamic instability and the mechanism of flutter". NACA Report 496, National Advisory Committee Aeronautics.

Trickey, S.T., Virgin, L.N. and Dowell, E.H., 2002. "The stability of limit-cycle oscillations in a nonlinear aeroelastic system". *Proceedings: Mathematical, Physical and Engineering Sciences*, Vol. 458, No. 2025, pp. 2203–2226.

Vasconcellos, R., Abdelkefi, A., Marques, F. and Hajj, M., 2012. "Representation and analysis of control surface freeplay nonlinearity". *Journal of Fluids and Structures*, Vol. 31, pp. 79 – 91. ISSN 0889-9746. doi:10.1016/j.jfluidstructs.2012.02.003.

9. RESPONSIBILITY NOTICE

The authors are solely responsible for the printed material included in this paper.

Appendix A. Matrices and Formulae

Matrices from Eq. (3),

$$\mathbf{M}_s = \begin{bmatrix} 1 & x_\alpha & x_\beta \\ x_\alpha^2 & r_\alpha^2 & r_\beta^2 + (c-a)x_\beta \\ x_\beta & r_\beta^2 + (c-a)x_\beta & r_\beta^2 \end{bmatrix}, \quad \mathbf{K}_s = \begin{bmatrix} \omega_h^2 & 0 & 0 \\ 0 & r_\alpha^2\omega_\alpha^2 & 0 \\ 0 & 0 & r_\beta^2\omega_\beta^2 \end{bmatrix},$$

$$\mathbf{f}_{nl}(\mathbf{x}_s(t)) = \begin{bmatrix} 0 \\ r_\alpha^2\omega_\alpha^2(C_\alpha\alpha^3(t) + Q_\alpha\alpha^5(t)) \\ 0 \end{bmatrix}, \quad \mathbf{M}_{nc} = -\frac{\rho b^2}{m}\begin{bmatrix} \pi & -\pi a & -T_1 \\ -\pi a & \pi\left(\frac{1}{8}+a^2\right) & -\left(T_7+(c-a)T_1\right) \\ -T_1 & 2T_{13} & -T_3/\pi \end{bmatrix},$$

$$\mathbf{K}_{nc} = -\frac{\rho U^2}{m}\begin{bmatrix} 0 & 0 & 0 \\ 0 & 0 & (T_4+T_{10}) \\ 0 & 0 & \left(T_5 - T_4T_{10}\right)/\pi \end{bmatrix}, \quad \mathbf{B}_{nc} = -\frac{\rho U b}{m}\begin{bmatrix} 0 & \pi & -T_4 \\ 0 & \pi\left(\frac{1}{2}-a\right) & T_1 - T_8 - (c-a)T_4 + T_{11}/2 \\ 0 & -2T_9 - T_1 + T_4\left(a-\frac{1}{2}\right) & -T_4T_{11}/(2\pi) \end{bmatrix},$$

$$\mathbf{B}_c = (c_0 - c_1 - c_3)\frac{\rho U b}{m}\begin{bmatrix} -2\pi & -2\pi\left(\frac{1}{2}-a\right) & -T_{11} \\ 2\pi\left(a+\frac{1}{2}\right) & 2\pi\left(\frac{1}{2}-a\right)\left(a+\frac{1}{2}\right) & T_{11}\left(a+\frac{1}{2}\right) \\ -T_{12} & -T_{12}\left(\frac{1}{2}-a\right) & -T_{11}T_{12} \end{bmatrix},$$

$$\mathbf{K}_c = (c_0 - c_1 - c_3)\frac{\rho U^2}{m}\begin{bmatrix} 0 & -2\pi & 2T_{10} \\ 0 & 2\pi\left(a+\frac{1}{2}\right) & 2T_{10}\left(a+\frac{1}{2}\right) \\ 0 & -T_{12} & -(T_{10}T_{12})/\pi \end{bmatrix},$$

$$\mathbf{A}_1 = \frac{\rho U^2}{m}\begin{bmatrix} -2\pi\left(c_1c_2 + c_3c_4\right) \\ 2\pi\left(a+\frac{1}{2}\right)\left(c_1c_2 + c_3c_4\right) \\ -T_{12}\left(c_1c_2 + c_3c_4\right) \end{bmatrix}, \quad \mathbf{A}_2 = \frac{\rho U^2}{m}\begin{bmatrix} -(2\pi/b)\left[Uc_2c_4(c_1+c_3)\right] \\ (2\pi/b)\left(a+\frac{1}{2}\right)\left[Uc_2c_4(c_1+c_3)\right] \\ -\left(T_{12}/b\right)\left[Uc_2c_4(c_1+c_3)\right] \end{bmatrix},$$

$$\mathbf{A}_3 = \begin{bmatrix} 1 & \left(\frac{1}{2}-a\right) & T_{11}/(2\pi) \end{bmatrix}, \quad \mathbf{A}_4 = \frac{U}{b}\begin{bmatrix} 0 & 1 & T_{10}/\pi \end{bmatrix}, \quad \mathbf{A}_5 = -\frac{U}{b}\left(c_2+c_4\right)\mathbf{I}_{1\times1}, \quad \mathbf{A}_6 = -\frac{U^2}{b^2}c_2c_4\mathbf{I}_{1\times1}$$

where $c_0 = 0$, $c_1 = 0.615$, $c_2 = 0.0455$, $c_3 = 0.335$ and $c_4 = 0.3$ are the coefficients of Wagner's function based on the Sears's approach (Vasconcellos *et al.*, 2012), and T_i are the so-called Theodorsen's constants given as,

$$T_1 = -\frac{2+c^2}{3}\sqrt{1-c^2} + c\cos^{-1}(c),\ T_3 = -\frac{1-c^2}{8}\left(5c^2+4\right) + \frac{1}{4}c\left(7+2c^2\right)\sqrt{1-c^2}\cos^{-1}(c) - \left(\frac{1}{8}+c^2\right)\left(\cos^{-1}(c)\right)^2,$$

$$T_4 = c\sqrt{1-c^2} - \cos^{-1}(c),\ T_5 = -\left(1-c^2\right) - \left(\cos^{-1}(c)\right)^2 + 2c\sqrt{1-c^2}\cos^{-1}(c),$$
$$T_7 = c\left(\frac{7+2c^2}{8}\right)\sqrt{1-c^2} - \left(\frac{1}{8}+c^2\right)\cos^{-1}(c),\ T_8 = -\frac{1}{3}\left(1+2c^2\right)\sqrt{1-c^2} + c\cos^{-1}(c),$$
$$T_9 = \frac{1}{2}\left[\frac{\sqrt{1-c^2}\left(1-c^2\right)}{3} + aT_4\right],\ T_{10} = \sqrt{1-c^2} + \cos^{-1}(c),\ T_{11} = (2-c)\sqrt{1-c^2} - (1-2c)\cos^{-1}(c),$$
$$T_{12} = (2+c)\sqrt{1-c^2} - (1+2c)\cos^{-1}(c),\ T_{13} = -\frac{1}{2}\left[T_7 + (c-a)\,T_1\right].$$

Matrices from Eq. (4),

$$\mathbf{M}_t = \begin{bmatrix} \mathbf{M}_s - \mathbf{M}_{nc} & \mathbf{0}_{3\times1} \\ \mathbf{0}_{1\times3} & \mathbf{I}_{1\times1} \end{bmatrix}, \quad \mathbf{B}_t = \begin{bmatrix} -\mathbf{B}_{nc} - \mathbf{B}_c & -\mathbf{A}_1 \\ -\mathbf{A}_3 & -\mathbf{A}_5 \end{bmatrix}, \quad \mathbf{K}_t = \begin{bmatrix} \mathbf{K}_s - \mathbf{K}_{nc} - \mathbf{K}_c & -\mathbf{A}_3 \\ -\mathbf{A}_4 & -\mathbf{A}_6 \end{bmatrix}.$$